Hindawi
International Journal of RF and Microwave Computer-Aided Engineering
Volume 2023, Article ID 6477987, 8 pages
https://doi.org/10.1155/2023/6477987

Research Article

A Compact Horizontal Coaxial to Ridge Gap Waveguide Transition for Ka-Band

Changjian Tao, Haidong Zheng, and Chuan Jin

Department of Security Instrument, First Research Institute of the Ministry of Public Security, Beijing 100048, China

Correspondence should be addressed to Changjian Tao; taocj@fiscan.cn

Received 6 March 2023; Revised 27 May 2023; Accepted 25 August 2023; Published 6 September 2023

Academic Editor: Khair Ayman Al Shamaileh

This paper presents a novel type of compact inline coaxial to ridge gap waveguide (RGW) transition, which covers the whole Ka frequency band. The structure connects with the connector's inner conductor through a rectangular probe directly. The probe is set in nail bed without any extra parts. Hence, a simple and compact transition comes to fruition at the circuit topology level. This transition can be considered as an inhomogeneous stripline, so the characteristic impedance can be analyzed similarly to the stripline. Beyond this, a mounting hole is drilled at rectangular probe to improve the robustness and convenience of assembly without welding or conductive adhesive bonding. To verify the performance of the proposed structure, a back-to-back transition is designed, fabricated, and measured. Measurement results achieve better than 20 dB return loss and about 0.15 dB insertion loss from 26.4 GHz to 40.4 GHz. It corresponds greatly with simulation results and bespeaks valuable in millimeter-wave applications.

1. Introduction

Hollow metal waveguide has been extensively used during the past few decades in radio frequency, especially in high power and low loss transmission circuits. The reason for the good performance is that the electromagnetic wave is enclosed in a metal cavity, and the dielectric along Poynting vector is air only. To combine the hollow waveguides to the final configuration, the different modules should always be manufactured separately and connected through screws or welds. But gaps and mismatches in the junction tend to worsen performance. These methods add complexity to the design and fabrication process and can be difficult to implement [1].

RGW technology was developed in [2, 3] to overcome the drawbacks of traditional waveguides [4]. It is based on the concept of artificial soft and hard surfaces in electromagnetics [5, 6], and the theories of it were presented in [2]. In RGW technology, an artificial magnetic conducting (AMC) surface, which is conveniently established by a bed of nails, is placed on either side of the metal ridge. The bed of nails is a development of soft and hard surface theory. As same as perfectly electric conducting (PEC) and perfectly magnetic conducting (PMC) strip grid in ideal soft and hard surfaces, it can mimic an anisotropic boundary conditions [7]. Waves of arbitrary polarization are allowed to propagate along the strip at the hard surface case and waves are stopped to propagate in other directions at the soft surface case [2]. The advantages of RGW can be described as wide broadband, low insertion loss, and self-package and can be easily integrated with other microwave chips or circuits.

Since it has the advantages mentioned above, many researchers have focused on its applications in recent years, such as antenna arrays [8, 9], power dividers [10, 11], diplexers [12, 13], and filters [14]. To connect the above modules or measure the performance of those devices, a transition between RGW and other conventional guiding structures, such as commercial coaxial connector or WR-28 waveguide, must be designed [15]. Since the commercial WR-28 waveguide always converts signal from coaxial to waveguide first, using a coaxial probe directly can simplify the structure and reduce cost. In [16], a bandwidth of 26% at 10 dB is achieved using the proposed transition covering a frequency range of 22.5 to 29 GHz. A wideband coaxial to RGW transition based on five sections of matching networks is introduced in [17], which can cover from 10 to 23 GHz with a very small reflection and low insertion loss.

Vertical transition is used in all of above structures. But in many situations, a horizontal transition is desired. In [18], a horizontal microstrip line to RGW transition using defected ground slot with 45% bandwidth in Ku-band is introduced. In [19], an ultrawideband inline coaxial to single ridge waveguide transition achieves better than 15 dB return loss from 11.5 to 33GHz. Compare with [18], this sort of structure does not require more headspace. But both of them use an extra part, which connects a 2.92 mm coaxial connector to a single ridge waveguide or a microstrip line before feeding the RGW. One common reason to avoid connecting coaxial connector with RGW directly is that this kind of transition is always responsible for limiting the bandwidth. This limitation, in many cases, is about one-third of the original unit cell bandwidth [17]. But for most applications, an ultrawideband is not necessary. Other properties, such as return loss, insertion loss, and dimension are also of concern.

Therefore, a compact horizontal coaxial to RGW transition is proposed in this article. The study find that an extra match part is unnecessary even if the running gamut of the device is the whole Ka-band. The advantage of connecting directly is that the complexity of manufacture and assembly can be appropriately reduced. Furthermore, the proposed structure is more robust in comparison to indirect connections. A back-to-back structure is designed to verify the feasibility of the proposed approach. Measurement and simulation are in accordance. It is shown that this kind of transition can easily be used in the system with a tight size requirement, which operates within the Ka-band.

2. RGW Structure Design and Simulation

The structure which is given in Figure 1 is possible to build a high-impedance surface in a broad bandwidth. As the transition focus on Ka-band, the band-gap range is designed from about 23 to 43 GHz. Pin height h initial dimension is approximately equal to $0.25\lambda_c$ (λ_c is the wavelength in center frequency), and any top view of the pin is square because the surface anisotropy does not add any direct advantage for application in RGW [20]. The initial dimensions of unit period p and pin width a can also be obtained according to [20]. The air gap g can be estimated by $f_{\text{high}} = c/2(h+g)$ [21]. The final g is optimized to 0.4 mm because the capacitance between the pin and top conductor increases with g decrease, which results in a wider bandgap [10, 22].

The simulated results of straight RGW are shown in Figure 2, in which S_{11} is below -25 dB and S_{12} is better than -0.06 dB in Ka-band that can be observed. The initial strip width w can be figured by the formula in (1) to implement RGW which has a 50-Ω characteristic impedance.

$$Z_{0,\text{RGW}} = \begin{cases} 60 \ln\left(\dfrac{8g}{w} + \dfrac{w}{4g}\right) & \dfrac{w}{g} < 1 \\ \dfrac{120\pi}{(w/g) + 1.393 + 0.667 \ln\left((w/g) + 1.444\right)} & \dfrac{w}{g} \geq 1 \end{cases}, \tag{1}$$

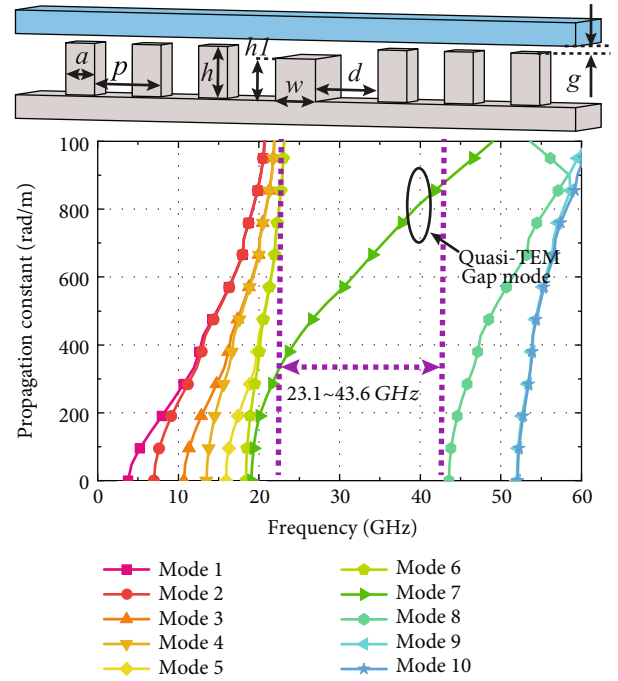

Figure 1: Design dimensions of RGW and dispersion diagram. Parameters: $g = 0.4$ mm, $a = 1.3$ mm, $h = 2.2$ mm, $h1 = 1.8$ mm, $p = 3$ mm, $w = 1.8$ mm, $d = 2.5$ mm.

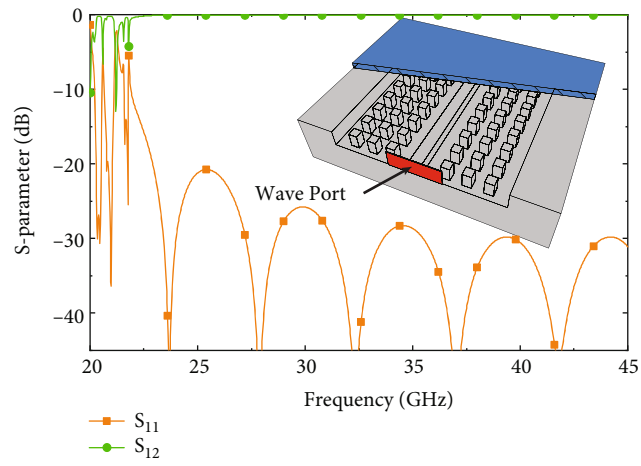

Figure 2: The S-parameters of straight RGW.

3. Design and Analysis of the Transition

3.1. Transition Structure Design. The proposed transition is shown in Figure 3. It is excited by coaxial connector, which has standard 50-Ω characteristic impedance. The inner conductor diameter is 0.3 mm. It is inserted into a mounting hole, which has a $e3$ diameter. The mounting hole compensates for assembly problem caused by tolerances in the length of the inner conductor.

To ensure 50-Ω characteristic impedance of coaxial line which constitute by the inner conductor of the connector and the probe via, R is designed as 0.69 mm. It can be calculated from the coaxial line impedance formula.

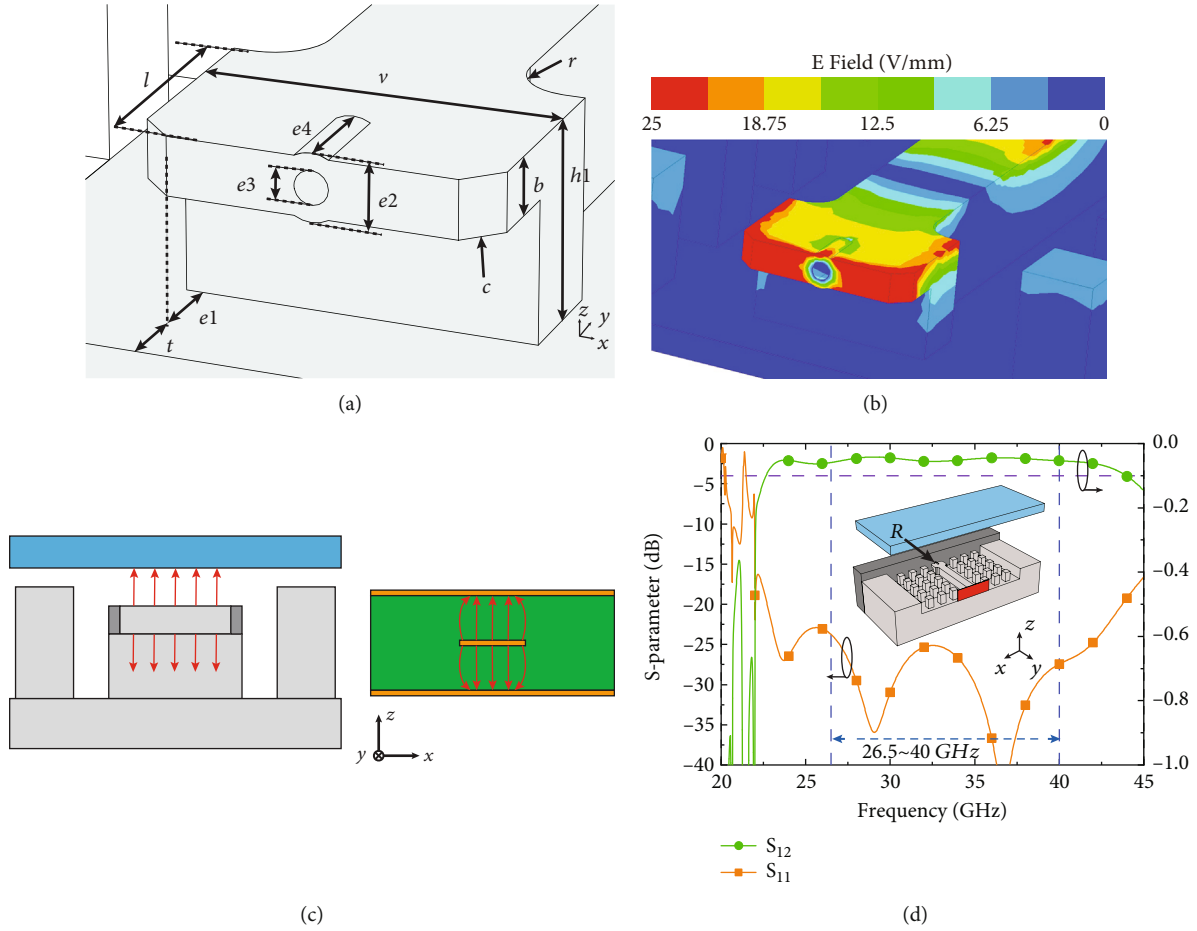

FIGURE 3: Structure and simulation results of the proposed transition. (a) Dimensions of the proposed transition. (b) Distribution of electric field on the transition structure. (c) Electric field lines of rectangular probe and stripline. (d) The simulation model and S-parameter results. Parameters: $l = 2.1$ mm, $v = 3.14$ mm, $b = 0.52$ mm, $t = 0.3$ mm, $c = 0.3$ mm, $r = 0.5$ mm, $e1 = 1.06$ mm, $e2 = 0.6$ mm, $e3 = 0.3$ mm, and $e4 = 0.9$ mm.

The initial dimension l can be designed as $0.25\lambda_c$. To enforce the electric field to upper ridge and weaken the electric at the bottom, a groove is added at the front of transition. This groove forms a rectangular probe with thickness and length of b and $e1$, respectively. The electric field distribution is shown in Figure 3(b). But as shown in Figure 4, the impedance matching performance is not acceptable even after optimization. To further reduce the capacitance between the rectangular probe and the side wall, a chamfer is placed at the most intensive electric field. It can intensify the resonance at high frequency.

Figure 3(c) shows the side view and electric field lines of the rectangular probe and the stripline. The front end of this probe is wrapped in dielectric on both the top and bottom sides. The electric field distributes between the top side of the probe and the metal cover, and the bottom side of the probe and the ground. It constitutes a kind of inhomogeneous stripline and has a very similar performance to the stripline. So the initial rectangular probe width v can be worked out by this modified stripline formulation (2). In traditional formula for the characteristic impedance of stripline, the thickness of the dielectric is considered as the distance between both ground planes. But in this design, the intensity of the electric field at the ground plane is negligible. It can be observed in Figure 3(b). So the thickness of the dielectric should be changed to twice the

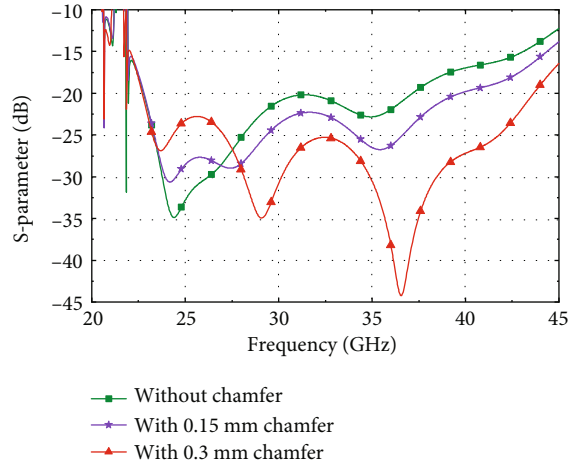

FIGURE 4: The effect of the chamfer on S_{11} of transition.

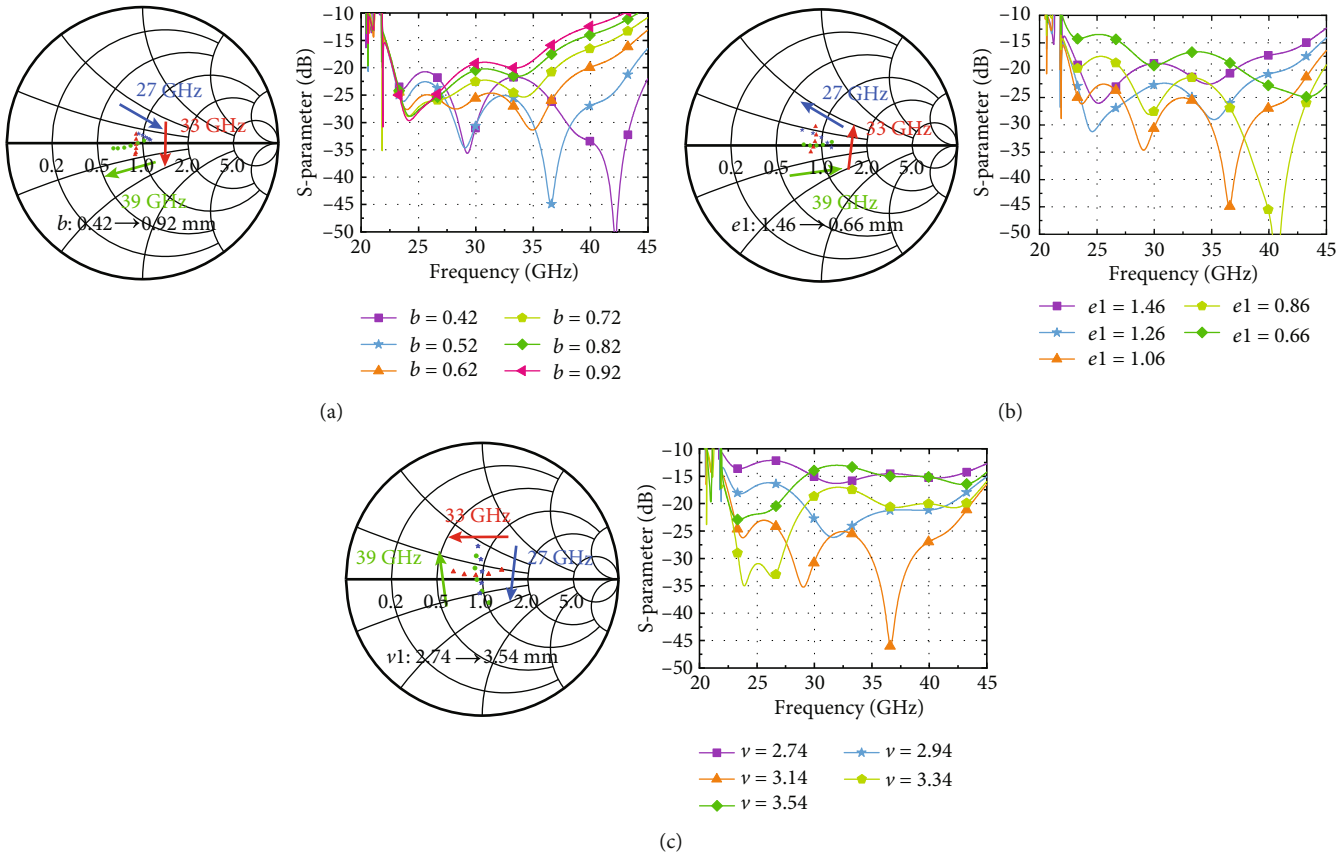

FIGURE 5: The Smith chart and *S*-parameters simulated results of *b* and *e*1 with different parameters. (a) The thickness of the rectangular probe *b*. (b) The length of the bottom of the rectangular probe *e*1. (c) The width of the rectangular probe *v*.

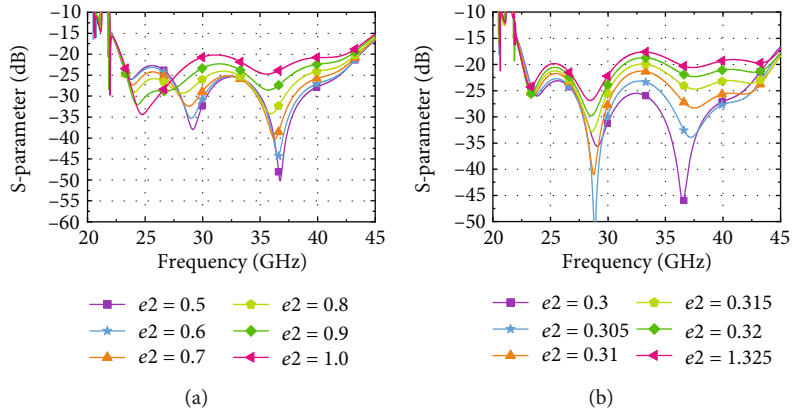

FIGURE 6: Simulated results of *e*2 and *e*3 with different parameters. (a) The diameter of cylindrical stiffener *e*2. (b) The diameter of the mounting hole *e*3.

distance between the metal cover and the probe, plus the thickness of the probe. Since the electric field transmits in air, the dielectric constant $\varepsilon_r = 1$. The width v can be calculated equal to 3.06 mm, and the final parameter is 3.14 mm after optimization.

$$Z_0 = \frac{30\pi}{\sqrt{\varepsilon_r}} \frac{2(g+h-h1)+b}{v+0.441[2(g+h-h1)+b]}. \quad (2)$$

The return loss below 20 dB from 22.75 to 43.66 GHz can be achieved. It can cover the whole Ka frequency band, and the insertion loss is less than 0.06 dB, as can be observed in Figure 3(d).

3.2. Analysis of Key Parameters. It can be seen from Figure 3(b) that the electric field is mainly concentrated on the rectangular probe, so the dimensions of the rectangular probe will significantly affect the performance of the

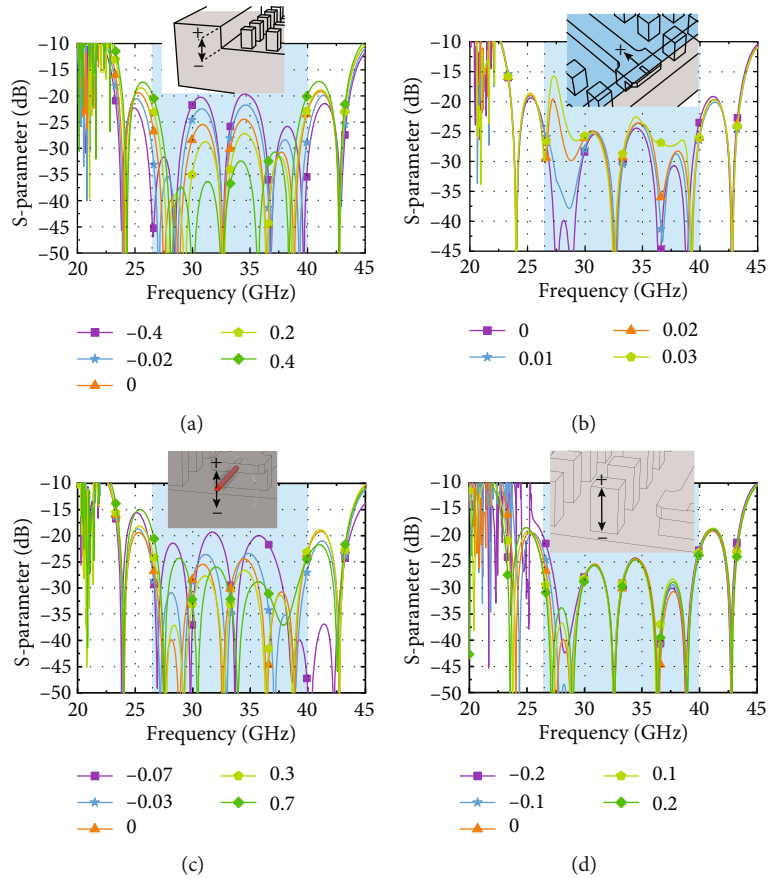

FIGURE 7: Evaluation of the effect of the tolerances. The inset illustrates the offsets rather than the design dimensions. (a) Evaluation of the effect on the distance between the metal cover and the ground. (b) Evaluation of the effect on the slit between the metal cover and the sidewall. (c) Evaluation of the effect on the misalignment of the coaxial probe. (d) Evaluation of the effect on the height of pins.

transition. The essence of the design is to optimize the series capacitance between the rectangular probe and side wall, and the parallel capacitance between the rectangular probe and ground. Figure 5(a) shows the parallel capacitance between the rectangular probe and ground scale up with the distance shrinkage at the center frequency. At the same frequency, this capacitance has a positive correlation with the area between the bottom side of the rectangular probe and the ground as Figure 5(b) shows. The change of parameters also varies the resistance mainly at both ends of the frequency, and they have opposite trends. The change of b affects the high-frequency of S-parameters largely, while $e1$ has a role in the entire frequency band. Figure 5(c) shows the width of the rectangular probe effect characteristic impedance at the center frequency. The reason is that the probe can be concerned as an inhomogeneous stripline. It displays a similar changing trend with stripline, which is the characteristic impedance turn down with the width increase.

As the thickness b of the rectangular probe is only 0.52 mm after optimization, a cylindrical stiffener that has a diameter $e2$ equal to 0.6 mm is placed to reinforce this structure to fulfill the requirement of a computer numerically controlled (CNC) technology. Figure 6 shows when the diameter $e2$ of cylindrical stiffener beyond 1 mm will deteriorate the S-parameter performance to above -20 dB. In addition, S_{11} is apt to worse with an increase in $e3$ because of poor contact. Therefore, the tolerance of $e3$ should be controlled as $0.3_{0}^{+0.01}$ to ensure that S_{11} is better than -20 dB.

3.3. Tolerance Analysis. The effect of different manufacturing and assembly errors will be evaluated in this section. To discuss the effect of crucial and subordinate parameters of manufacturing and assembly, four parameters are selected.

Firstly, the crucial assembly parameter is the distance between the cover and the ground. It is because this parameter will change the capacitance between the transition and metal cover. To evaluate the effect of this air gap, the distance has been swept around the nominal value. The results are shown in Figure 7(a). The return loss will be worse than 20 dB when the deviation is over -0.04 mm, and the bandwidth will tape to less than 13.5 GHz when the deviation is over 0.04 mm. Figure 7(b) shows another crucial parameter of manufacturing, which is the length of the metal cover. The reason is that the electric field at the edge of the metal cover is dramatically more intensive than in other places. When a 0.02 mm slit appears between the cover and sidewall, the degradation of return loss is unacceptable. Considering the capability of CNC and the requirement of the transition's performance, the tolerances of crucial

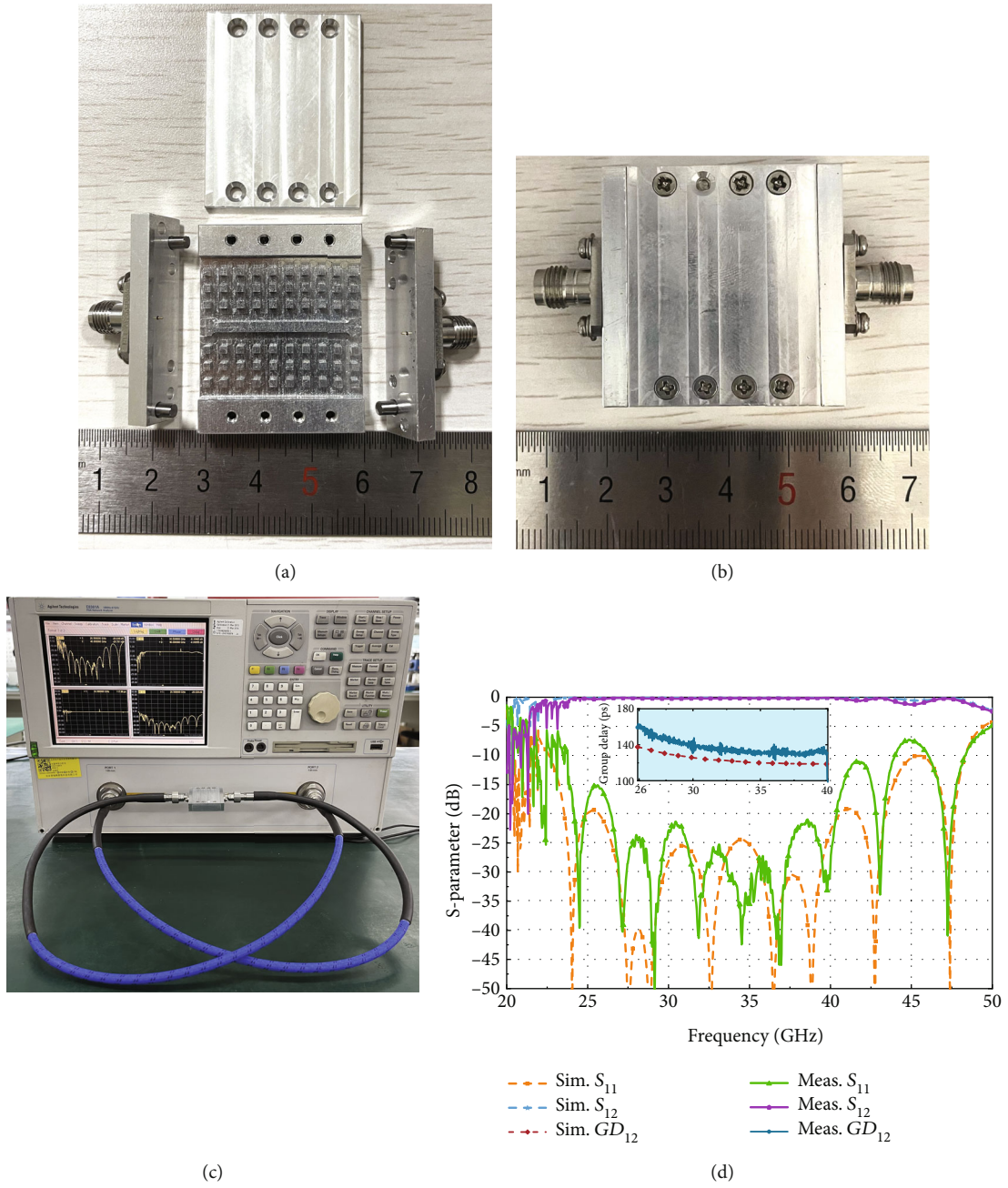

FIGURE 8: Photographs of the back-to-back transition and measurement results. (a) Transition before assembly. (b) Transition after assembly. (c) Setup and results of the measurement of the assembled transition. (d) Measurement and simulation results.

parameters should be controlled at least as ±0.02 mm in Ka-band. In this work, these tolerances are controlled as ±0.01 mm.

In addition, the misalignments of the coaxial probe have been displayed in Figure 7(c). When the offset reaches 0.07 mm, either S_{11} or the bandwidth is unsatisfactory. It is mainly because of the lost of symmetry for the coaxial transmission line. Finally, in any cases shown in Figure 7(d), the return loss is below 20 dB in operation band. It can be observed that when the height of the pin is swept around the nominal value, the transition behavior remains hardly unaffected. Therefore, the dimensions of the pins are subordinate to manufacturing. [23] has also discussed this phenomenon. In a word, the tolerances of subordinate parameters can be controlled as ±0.05 mm. In this work, these tolerances are controlled as ±0.03 mm.

4. Measurement Results

In order to test the performance of the proposed structure, a back-to-back transition module is realized by CNC technology. Back-to-back measurements are widely used for similar transitions. The reason for this setup can be explained by the symmetrical structure of the back-to-back transition. It is

Table 1: Dimensions of the transition.

Parameter	Description	Design (mm)	Fabricated (mm)
a	Pin width	1.3	1.29
h	Pin height	2.2	2.18
$p-a$	Pin gap	1.7	1.71
$g+h$	Cover-to-ground length	2.6	2.59
v	Rectangular probe width	3.14	3.13
b	Rectangular probe thickness	0.52	0.51
$e2$	Cylindrical stiffener diameter	0.6	0.57
$h1$	RGW height	1.8	1.8
w	RGW width	1.8	1.83

Table 2: Comparisons with related works.

Ref.	Freq (GHz)	Insertion loss	Return loss	Structural complexity	Size ($l \times w \times h$) (λ_c)	Extra part
[17]	10-23 78.8%	≈0.15 dB	>18 dB	Five step matching + three step back cavity	$2.3 \times 0.89 \times 0.14$	Yes
[18]	11.8-18.8 45.8%	≈0.5 dB	>10 dB	Microstrip line + three step matching	$1 \times 1.3 \times 0.28$	Yes
[19]	15-40 90.9%	≈0.2 dB (Sim)	>15 dB	Rectangular probe + cavity + screws	$2.3 \times 0.89 \times 0.48$	Yes
This work	26.4-40.4 41.9%	≈0.18 dB	>20 dB	Rectangular probe	$0.27 \times 0.35 \times 0.2$	No

convenient to measure the performance, such as insertion loss, of the entire DUT after calibrating the vector network analyzer (VNA) to evaluate the performance of a single side. All components of the real object before and after assembly are shown in Figure 8. Two dowels on each side wall are installed to ensure that the center of the probe is aligned with the center of the mounting hole. They are all fabricated from aluminum and connected by fixing screws. It is not necessary to weld or use conductive adhesive to assemble the connector and the transition.

This measurement is done using Agilent Technologies E8361A VNA as shown in Figure 8(c). The effect of connectors has been calibrated. As shown in Figure 8(d), the measured S_{11} is better than -20 dB in 26.4–40.4 GHz. The fluctuation of S_{12} is from -0.09 dB to -0.26 dB in the same frequency band as above. Compare with measurement, the fluctuation of S_{12} is from -0.08 dB to -0.11 dB in simulation. A typical value of group delay response of measurement and simulation is 136.9 ps and 121.8 ps at 33 GHz. There is about a 0.9 GHz bandwidth decrease in measured S_{11} and a 0.08 dB worsen in S_{12} than simulated. The worst value of simulation and measurement of S_{11} in the whole Ka-band is -23.02 dB and -20.65 dB, respectively. This value is deteriorated by 2.37 dB.

These differences have some common reasons. Firstly, the surface roughness cannot be exactly estimated in software. Furthermore, tolerances are introduced in the manufacturing process, and inaccurate alignment during assembly can cause differences in results. Some dimensions of the transition can be seen in Table 1. The measurement is done using 3D Family NV300 3D vision measuring instrument. These dimensions are able to meet the aforementioned tolerance requirements, so the deterioration of S_{11} is in an acceptable range.

A comparison with related works is summarized in Table 2. The designed transition offers the most simple structural complexity and the best performance of return loss without any extra part. Note that the insertion loss level is assessed for double transition and includes the transmission line which connects the double transition in [18] and this work. In [17, 19], the back-to-back transitions are connected directly without a transmission line, and the insertion loss in [19] is the simulation result.

5. Conclusion

This article presents a new type of compact horizontal coaxial to RGW transition. The features of the developed design are concise and compact, which cover the entire Ka-band without an externally independent fitting transition structure. A reinforcement structure is placed at the forefront of the rectangular probe, and some key parameters are analyzed. Measurement results approach a good agreement with simulations and show the robustness of the capability of this transition, which can be used in many different sorts of RGW engineering in the Ka-band.

Data Availability

The data that support the findings of this study are available from the corresponding author upon reasonable request.

Conflicts of Interest

The authors declare that they have no conflicts of interest.

Acknowledgments

This work was supported by the Central Public-Interest Scientific Institution Basal Research Fund of China under grant A23609GY.

References

[1] N. Jastram, M. A. Altarifi, L. Boskovic, and D. S. Filipovic, "On the split-block realization of millimeter-wave ridge waveguide components," *IEEE Microwave and Wireless Components Letters*, vol. 28, no. 4, pp. 296–298, 2018.

[2] P.-S. Kildal, E. Alfonso, A. Valero-Nogueira, and E. Rajo-Iglesias, "Local metamaterial-based waveguides in gaps between parallel metal plates," *IEEE Antennas and Wireless Propagation Letters*, vol. 8, pp. 84–87, 2009.

[3] P.-S. Kildal, "Three metamaterial-based gap waveguides between parallel metal plates for mm/submm waves," in *2009 3rd European Conference on Antennas and Propagation*, pp. 28–32, Berlin, Germany, 2009.

[4] S. Peng, Y. Pu, Z. Wu, X. Chen, and Y. Luo, "Embedded bed of nails with robustness suitable for broadband gap waveguide technology," *IEEE Transactions on Microwave Theory and Techniques*, vol. 69, no. 12, pp. 5317–5326, 2021.

[5] P.-S. Kildal, "Definition of artificially soft and hard surfaces for electromagnetic waves," *Electronics Letters*, vol. 24, no. 3, pp. 168–170, 1988.

[6] P.-S. Kildal, "Artificially soft and hard surfaces in electromagnetics," *IEEE Transactions on Antennas and Propagation*, vol. 38, no. 10, pp. 1537–1544, 1990.

[7] M. G. Silveirinha, C. A. Fernandes, and J. R. Costa, "Electromagnetic characterization of textured surfaces formed by metallic pins," *IEEE Transactions on Antennas and Propagation*, vol. 56, no. 2, pp. 405–415, 2008.

[8] J. Liu, F. Yang, K. Fan, and C. Jin, "Unequal power divider based on inverted microstrip gap waveguide and its application for low sidelobe slot array antenna at 39 GHz," *IEEE Transactions on Antennas and Propagation*, vol. 69, no. 12, pp. 8415–8425, 2021.

[9] H. Attia, A. A. Kishk, M. A. Abdalla, S. Gaya, A. Hamza, and A. Mahmoud, "Ridge gap waveguide antenna array with improved mutual isolation for millimeter wave applications," *International Journal of RF and Microwave Computer-Aided Engineering*, vol. 31, no. 11, Article ID e22831, 2021.

[10] B. Ahmadi and A. Banai, "A power divider/combiner realized by ridge gap waveguide technology for millimeter wave applications," in *2016 Fourth International Conference on Millimeter-Wave and Terahertz Technologies (MMWaTT)*, pp. 5–8, Tehran, Iran, 2016.

[11] J.-C. S. Chieh, "A substrate-less microwave power-combining module utilizing ridge gap waveguide," *IEEE Microwave and Wireless Components Letters*, vol. 28, no. 11, pp. 972–974, 2018.

[12] D. Zarifi, A. Shater, A. Ashrafian, and M. Nasri, "Design of Ku-band diplexer based on groove gap waveguide technology," *International Journal of RF and Microwave Computer-Aided Engineering*, vol. 28, no. 9, Article ID e21487, 2018.

[13] L.-F. Wang, S.-B. Xue, Z.-Y. Mao, and M. Li, "Compact dual-band inverted-microstrip ridge gap waveguide diplexer," *International Journal of RF and Microwave Computer-Aided Engineering*, vol. 31, no. 10, Article ID e22829, 2021.

[14] J. Chen, D. Shen, X. Zhang, and Y. Sa, "Integrated substrate groove gap waveguide and application for filter design," *International Journal of RF and Microwave Computer-Aided Engineering*, vol. 31, no. 11, Article ID e22830, 2021.

[15] I. Afifi, M. M. M. Ali, and A.-R. Sebak, "Analysis and design of a wideband coaxial transition to metal and printed ridge gap waveguide," *Ieee Access*, vol. 6, article 70698, 2018.

[16] M. Al Sharkawy and A. A. Kishk, "Design of waveguide to ridge gap waveguide transition using probe excitation," in *The 8th European Conference on Antennas and Propagation (EuCAP 2014)*, pp. 946–949, The Hague, Netherlands, 2014.

[17] S. I. Shams and A. A. Kishk, "Wideband coaxial to ridge gap waveguide transition," *IEEE Transactions on Microwave Theory and Techniques*, vol. 64, no. 12, pp. 4117–4125, 2016.

[18] B. Molaei and A. Khaleghi, "A novel wideband microstrip line to ridge gap waveguide transition using defected ground slot," *IEEE Microwave and Wireless Components Letters*, vol. 25, no. 2, pp. 91–93, 2015.

[19] M. A. Nasr and A. A. Kishk, "Wideband inline coaxial to ridge waveguide transition with tuning capability for ridge gap waveguide," *IEEE Transactions on Microwave Theory and Techniques*, vol. 66, no. 6, pp. 2757–2766, 2018.

[20] E. Rajo-Iglesias and P.-S. Kildal, "Numerical studies of bandwidth of parallel-plate cut-off realised by a bed of nails, corrugations and mushroom-type electromagnetic bandgap for use in gap waveguides," *IET Microwaves, Antennas & Propagation*, vol. 5, no. 3, pp. 282–289, 2011.

[21] S. I. Shams and A. A. Kishk, "Printed texture with triangle flat pins for bandwidth enhancement of the ridge gap waveguide," *IEEE Transactions on Microwave Theory and Techniques*, vol. 65, no. 6, pp. 2093–2100, 2017.

[22] D. Sun and J. Xu, "A novel iris waveguide bandpass filter using air gapped waveguide technology," *IEEE Microwave and Wireless Components Letters*, vol. 26, no. 7, pp. 475–477, 2016.

[23] J. M. Pérez-Escudero, A. E. Torres-Garca, R. Gonzalo, and I. Ederra, "A Chebyshev transformer-based microstri-to-groove-gap-waveguide inline transition for MMIC packaging," *IEEE Transactions on Components, Packaging and Manufacturing Technology*, vol. 9, no. 8, pp. 1595–1602, 2019.